International Forum on Aeroelasticity and Structural Dynamics
IFASD 2017
25-28 June 2017 Como, Italy

A NONLINEAR FREQUENCY DOMAIN AERODYNAMIC MODEL FOR CONTINUOUS TURBULENCE ENCOUNTER BASED ON FUNCTIONAL SERIES EXPANSION

David Quero[1] **and Wolf Krüger**[1]

[1]DLR (German Aerospace Center)
Institute of Aeroelasticity
Bunsenstr. 10, 37073 Göttingen, Germany
David.QueroMartin@DLR.de, Wolf.Krueger@DLR.de

Keywords: ROM, nonlinear, Volterra series, gust encounter, continuous turbulence

Abstract: In this paper a nonlinear Reduced Order Model (ROM) for a frequency domain aerodynamic model based on functional or Volterra series expansion is presented. It relies on the numerical identification of the higher order Volterra Kernels by a continuous time impulse method and the transformation into the frequency domain with multidimensional Fourier transforms. This frequency domain ROM allows the nonlinear computation of the output power spectra as function of the input power spectra, showing an independence on the randomness of the phase for random Gaussian stationary processes. Gust and continuous turbulence encounters are considered for a rigid wing empennage configuration flying in the transonic regime. Results obtained with the nonlinear frequency domain ROM are compared against CFD Euler computations for a discrete gust case showing a very good agreement. For continuous turbulence encounters the influence of the nonlinearity in the root mean square of the output when increasing the turbulence intensity is considered, showing a cubic dependency with the root mean square value of the turbulence for a second order Volterra series expansion. Additionally, convergence issues experienced by full-order CFD simulations when the turbulence intensity is increased are pointed out.

1 INTRODUCTION

Dynamic loads due to atmospheric disturbances are of capital importance when designing and sizing an aircraft. There are very well established linear methods to compute the aerodynamic loads, both in the frequency and the time domain, which properly represents the physics for subsonic cases, where the aerodynamic remains linear. Probably the best known is the Doublet-Lattice Method (DLM) in the frequency domain [1], which solves the unsteady compressible potential equation. In order to consider the compressible effects inherent to the transonic region, linear(ized) aeroelastic ROMs have been presented by several authors. The term linear(ized) refers to the fact that the nonlinear nature of the steady aerodynamic state is taken into account and only the unsteady incremental aerodynamic effects around the steady state are considered to be linear. A review on linear(ized) aeroelastic ROMs including Proper Orthogonal Decomposition (POD) and Eigensystem Realisation Algorithm (ERA) as presented by Silva [2] is given by Ripepi [3] and Quero [4]. The proposed aeroelastic ROM by Quero [4] makes use of a reduced number of high-fidelity reference computations. A review on nonlinear aerodynamic ROM methods including Volterra series, indicial functions, Harmonic Balance (HB), Taylor series

expansion, surrogate-based and neural networks approaches is given by Ripepi [3]. Quero [4] presents an extension for the nonlinear aerodynamic effects when encountering discrete gusts. However and to the best of the author's knowledge a nonlinear aerodynamic ROM for general atmospheric disturbance excitations in the frequency domain has not yet been presented.

In this work the analysis is restricted to vertical disturbances but can be extended to disturbances acting on different spatial directions. The presented ROM is able to notably improve the nonlinear aerodynamic response prediction when compared to the linear(ized) methods and additionally is able to predict a nonlinear dependency of the aerodynamic output root mean square (rms) values as function of the turbulence rms where full-order simulations fail to converge. These predictions are obtained in a computational time up to four orders of magnitude smaller than that required by the high-fidelity methods.

2 FUNCTIONAL SERIES

In this work the (nonlinear) aerodynamic system under consideration is given by Eq. 1, which represents the *state equation* after spatial discretization of the flow equations, where $\mathbf{y}_w$ represents the flow variables, $\mathbf{u}_h$ and $\dot{\mathbf{u}}_h$ the generalized structural deformation and its time derivative and $\mathbf{v}_d$ the gust velocity vector at each considered node in the flow. The system input is defined as $\mathbf{u} = [\mathbf{u}_h^T \, \dot{\mathbf{u}_h}^T \, \mathbf{v}_d^T]^T$. Note that these three components are dealt separately for the sake of clarity. Also, the explicit dependency on the Reynolds number Re_∞ has been omitted, as its value is assumed to be known in the case that viscous effects are considered. The dependency on the steady angle of attack α_s is shown in order to highlight the dependency of the proposed methods with the steady state. Both parameters M_∞ and α_s specify boundary conditions for the spatial discretized flow equations.

$$\dot{\mathbf{y}}_w\left(t, M_\infty, \alpha_s\right) = \mathbf{F}\left(\mathbf{y}_w\left(t\right), \mathbf{u}_h\left(t\right), \dot{\mathbf{u}}_h\left(t\right), \mathbf{v}_d\left(t\right), M_\infty, \alpha_s\right) \tag{1}$$

The function $\mathbf{F}$ does not depend explicitly on time, as the Navier-Stokes equations do not have any coefficients that are explicit functions of time. As stated by Silva [5] the Navier-Stokes equations are, by definition, time invariant. A condition of consistency requires that, in the limit, the discretized system approaches the original continuous time system. Therefore, given appropriate discretization and convergence of the residual (error), the discretized Navier-Stokes are time invariant as well.

The *output equation* provides the vector of aerodynamic quantities $\mathbf{P}_g$ at the different spatial locations, see Eq. 2. The vector $\mathbf{P}_g$ represents the aerodynamic loads acting at the structural nodes. Under the assumption of small structural displacements the dependency of the function $\mathbf{G}$ may be reduced to $\mathbf{P}_g\left(t, M_\infty, \alpha_s\right) = \mathbf{G}\left(\mathbf{y}_w\left(t\right), M_\infty, \alpha_s\right)$.

$$\mathbf{P}_g\left(t, M_\infty, \alpha_s\right) = \mathbf{G}\left(\mathbf{y}_w\left(t\right), \mathbf{u}_h\left(t\right), \dot{\mathbf{u}}_h\left(t\right), \mathbf{v}_d\left(t\right), M_\infty, \alpha_s\right) \tag{2}$$

Now the Volterra or functional series expansion for a general Single Input Multiple Output (SIMO) is described. The Volterra series representation can be used to described systems with fading memory [6] and which do not contain subharmonics [7]. Some modification on the regular Volterra representation allows its extension to include subharmonic components [8] and are

not considered in this work. In theory any system which can be described by a time invariant Ordinary Differential Equation (ODE) can be described by a Volterra series, as any time invariant ODE can be converted into an integral equation and solved for its Volterra kernels [9, 10].

For a nonlinear Single Input Multi Output (SIMO) system stable at the zero equilibrium point and which can be described in the neighborhood of the equilibrium point by the Volterra series, the output component $y_j(t)$ fulfills Eq. 3, where $u(t)$ is the system input and $h_{nj}(\tau_1, ..., \tau_n)$ is the *n*th-order Volterra kernel for the output component j, where $j = 1, ..., N_y$, with N_y the number of outputs. The maximum order of nonlinearity taken into account is denoted by N_n. In this work $N_n = 2$ and thus a second order Volterra or functional series expansion is considered.

$$y_j(t) = \sum_{n=1}^{N_n} y_{nj}(t) = \sum_{n=1}^{N_n} \int_{-\infty}^{\infty} ... \int_{-\infty}^{\infty} h_{nj}(\tau_1, ..., \tau_n) \prod_{k=1}^{n} u(t - \tau_k) \, d\tau_k \tag{3}$$

When the system is excited by the general input $u(t) = (1/2\pi) \int_{-\infty}^{\infty} u(\omega) \, e^{i\omega t} d\omega$ with frequency content $u(\omega)$, the homogeneous term $y_{nj}(t)$ is given by Lang et al. [11],

$$y_{nj}(t) = \frac{1}{(2\pi)^n} \int_{-\infty}^{\infty} ... \int_{-\infty}^{\infty} y_{nj}(\omega_1, ..., \omega_n) \, e^{i(\omega_1 + \cdots + \omega_n)t} d\omega_1 ... d\omega_n$$

where $y_{nj}(\omega_1, ..., \omega_n) = H_{nj}(\omega_1, ..., \omega_n) \prod_{k=1}^{n} u(\omega_k)$. The function $H_{nj}(\omega_1, ..., \omega_n)$ is referred to as frequency domain Volterra kernel. The Volterra kernels of higher order $h_{nj}(\tau_1, ..., \tau_n)$ are not unique and several forms are available. In this work, the symmetric form is considered.

By applying the transformation of variables $\omega = \omega_1 + \cdots + \omega_n$ the term $y_{nj}(t)$ can be expressed as $y_{nj}(t) = (1/(2\pi)^n) \int_{-\infty}^{\infty} y_{nj}(\omega) \, e^{i\omega t} d\omega$, where $y_{nj}(\omega)$ is given in Eq. 4 according to Lang et al. [11]. This transformation of variables is referred to as association of variables when considering the multidimensional Laplace transform as described by Lebnath et al. [12]. The term $y_{nj}(\omega)$ defines the frequency domain content of the output of the homogeneous system.

$$y_{nj}(\omega) = \frac{1}{(2\pi)^{n-1}} \int_{-\infty}^{\infty} ... \int_{-\infty}^{\infty} y_{nj}(\omega_1, ..., \omega - \omega_1 - \cdots - \omega_{n-1}) \, d\omega_1 ... d\omega_{n-1} \tag{4}$$

2.1 Continuous time impulse method for numerical Kernel identification

A review on the application of the Volterra theory to nonlinear aeroelastic systems is given by Silva [13]. Most of the aeroelastic applications including Volterra series expansion have included the consideration of structural nonlinearities, as done by Marzocca et al. [14], where the Volterra kernels are derived analytically in the frequency domain with the harmonic probing method [15]. An analytical form cannot in general be obtained when considering the aerodynamic contribution of the aeroelastic system and thus identification algorithms for the determination of the Volterra kernels must be used. Balajewicz et al. [16] and Khawar et al. [17] considered simultaneous heave and pitch aerodynamic excitations and computed the nonlinear response with the Volterra series expansion in the time domain. In this work the aerodynamic contribution of the aeroelastic system due to atmospheric disturbances is considered and a frequency domain formulation of the Volterra series is presented.

There are several possibilities in order to identify the system Volterra kernels, as described by Prazenica [10]. Balajewicz et al. [16] used training inputs from the full-order system and a standard least squares approach. Lee and Schetzen [18] proposed white noise and cross correlation methods based on the Wiener orthogonalization of the Volterra series [19]. Prazenica [10] and Kurdila et al. [20] approximated the Volterra kernels with wavelets functions. Different sets of basis functions are also available, among them Laguerre polynomials [21], decaying exponentials [22] and artificial neural networks as applied by Wray et al. [23]. The Volterra kernels can be measured by applying impulses to the system. Silva [24] used this approach for discrete time systems by applying unit sample inputs, the discrete analog to impulse inputs, to certain CFD models.

The application of discrete impulses for the Volterra kernels identification may introduce some numerical errors, as explained by Raveh [25]. A discussion on step inputs for the identification of the Volterra kernels can be found in Schetzen [26]. Additionally, when applied to flow solvers, the high gradient produced by the discrete impulse can lead to convergence issues due to the time derivative terms as described by Silva [27]. Thus, a method for identification of the Volterra kernels using smooth discrete impulse signals is preferred when dealing with numerical solvers and is thus applied in this work. This approach is denoted as continuous time impulse method as proposed by Milanese et al. [28], where the influence of the impulse amplitude was considered. In this work additionally the input shape is considered. Note that the derivative of the unit discrete impulse tends towards infinity at the initial time while the smooth impulse has finite values during the duration of the pulse. The continuous time impulse method assumes that the nonlinear system representation in the frequency domain is the same for both the discrete and the narrow smooth signal. It seems then clear that the smooth pulse signal must be narrow in order to have a shape very close to that of the ideal discrete pulse. Fig. 1 shows a comparison between the unit discrete impulse and the smooth impulse signal used as input.

The amplitude of the input impulse used for the Volterra kernel identification is dependent on the kernel degree. In particular the input amplitude used to identify the first order is smaller than the one used for the second order, where some level of the system nonlinearity must be present. For the first order the input is given in Eq. 5, where A_1 can be chosen $A_1 \ll 1$ in order to extract the linear contribution and $\delta_{se}(t)$ is the smooth impulse of unit amplitude with t_{max} the impulse duration as proposed by Marques et al. [29].

$$u_1(t) = A_1 \delta_{se}(t), \quad \delta_{se}(t) = \begin{cases} 4\left(\frac{t}{t_{max}}\right)^2 \exp\left(2 - \frac{1}{1-(t/t_{max})}\right), & 0 \leq t \leq t_{max}, \\ 0, & t \geq t_{max} \end{cases} \tag{5}$$

The input signal for the *n*th-component nonlinearity is defined in Eq. 6 as a linear combination of n delayed smooth impulses.

$$u_n(t) = A_n \left[\delta_{se}(t) + \sum_{k=1}^{n-1} \delta_{se}(t - \triangle t_k) \right] \tag{6}$$

In Eq. 6 $\triangle t_i$ is a time delay between the different impulse components and A_n is a factor dependent on the kernel degree. The maximum input amplitude is achieved when the impulse $\delta_{se}(t)$ is applied n times simultaneously ($\delta t_i = 0$ for all $i = 1, ..., n-1$) and is equal to nA_n. If

$A_n = A_{n-1}$ the maximum input amplitude increases linearly with n. Typically $A_n/A_{n-1} > 1$ so that the input is progressively increased in order to include more nonlinear behaviour. However the quotient A_n/A_{n-1} must be carefully chosen, as increasing values may produce shadowing effects from the higher order kernels in the one to be identified as pointed out by Milanese et al. [28].

Next the application of the continuous time impulse method to the identification of the first and higher order Volterra kernels for Single Input Multiple Output (SIMO) systems is described.

First order

The continuous time impulse method is an extension of the scheme to compute the transfer function for linear systems by means of an smooth impulse input signal, see Eq. 7 as provided by Marques et al. [30]. There $u_1(t)$ represents the smooth impulse imposed as input to the system, see Eq. 5, and $\bar{h}_{1j}(t)$ the corresponding dynamic response to $u_1(t)$ (obtained by direct numerical simulation) for the component y_j of the output vector $\mathbf{y}$, where $j = 1, ..., N_y$. As pointed out above both the amplitude and shape of the impulse signal are taken into account through the term $\int_{-\infty}^{\infty} u_1(t) e^{-i\omega t} dt$. The first kernel $h_{1j}(t)$ can be obtained by means of the inverse Fourier transform applied to the identified transfer function or first order frequency domain Volterra kernel $H_{1j}(\omega)$.

$$H_{1j}(\omega) = \frac{\int_{-\infty}^{\infty} \bar{h}_{1j}(t) e^{-i\omega t} dt}{\int_{-\infty}^{\infty} u_1(t) e^{-i\omega t} dt}, \quad h_{1j}(t) = \frac{1}{2\pi} \int_{-\infty}^{\infty} H_{1j}(\omega) e^{i\omega t} d\omega \tag{7}$$

In order to avoid numerical issues when applying the identified first order transfer function $H_{1j}(\omega)$ the frequency values satisfying the condition $|u_1(\omega)| / max(|u_1(\omega)|) \geq \omega_\epsilon$ are considered, where the tolerance ω_ϵ has been set to $\omega_\epsilon = 0.1$. At the frequency $\tilde{\omega}_1$ the equality condition is reached. For frequencies $|\omega| > \tilde{\omega}_1$ the first order transfer function $H_{1j}(\omega)$ is set to zero.

Higher order

When considering higher order terms in the Volterra or functional series Eq. 8 is used for the determination of the frequency domain Volterra kernels $H_{nj}(\omega_1, ..., \omega_n)$, where $\bar{h}_{nj}(t_1, ..., t_n)$ represents the dynamic response to $u_n(t)$ given in Eq. 6 from a direct simulation of the nonlinear system. Note that $\bar{h}_{nj}(t_1, ..., t_n) \neq y_{nj}(t_1, ..., t_n)$, where $y_{nj}(t_1, ..., t_n)$ is the *n*th-component y_j of the system response to the input $u_n(t)$. Note that the multidimensional input $u_n(t_1, ..., t_n)$ is formed by smooth pulses and not with unit discrete pulses. The Volterra kernels in time domain $h_{nj}(t_1, ..., t_n)$ can be obtained with the inverse multidimensional Fourier transform, $h_{nj}(t_1, ..., t_n) = (1/(2\pi)^n) \int_{-\infty}^{\infty} ... \int_{-\infty}^{\infty} H_{nj}(\omega_1, ..., \omega_n) e^{i(\omega_1 + \cdots + \omega_n)t} d\omega_1 ... d\omega_n$.

$$H_{nj}(\omega_1, ..., \omega_n) = \frac{\int_{-\infty}^{\infty} ... \int_{-\infty}^{\infty} \bar{h}_{nj}(t_1, ..., t_n) e^{-i(\omega_1 + \cdots + \omega_n)t} dt_1 ... dt_n}{\prod_{k=1}^{n} \int_{-\infty}^{\infty} u_n(t) e^{-i\omega_k t} dt} \tag{8}$$

For a second order approximation via Volterra or functional series the term $\bar{h}_{2j}(t_1, t_2)$ is given by Silva [24],

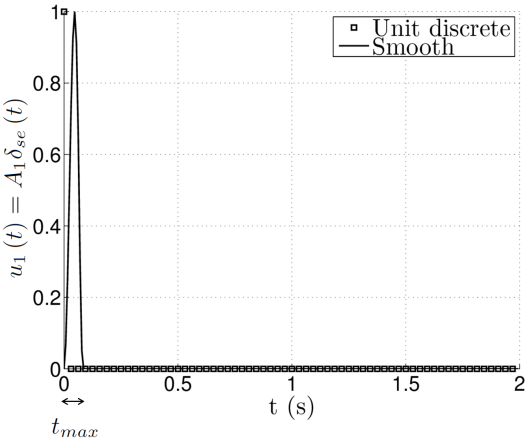

Figure 1: Continuous time impulse ($A_1 = 1$) input $u_1(t) = A_1\delta_{se}(t)$.

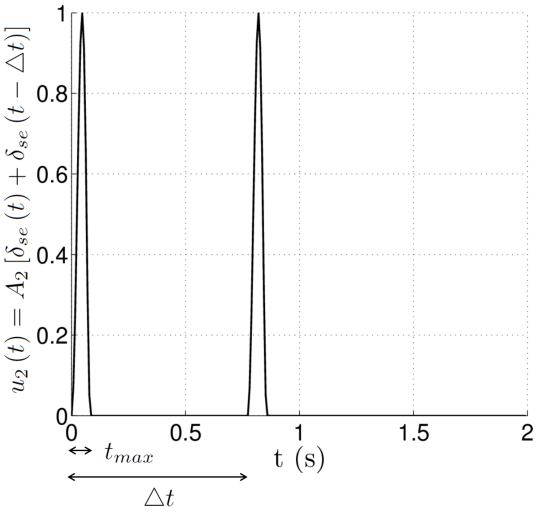

Figure 2: Continuous time impulse ($A_2 = 1$) input $u_2(t) = A_2[\delta_{se}(t) + \delta_{se}(t - \triangle t)]$.

$$\bar{h}_{2j}(t_1, t_2) = \frac{1}{2}\left[y_{2j}(t_1, t_2) - y_{1j}(t_1) - y_{1j}(t_2)\right]$$

, where y_{2j} represents the output to an input $u_2(t_1) = A_2[\delta_{se}(t_1) + \delta_{se}(t_2)]$, $y_{1j}(t_1)$ the output to an input $u_1(t_1) = A_1\delta_{se}(t_1)$ and $y_{1j}(t_2)$ the output to an input $u_1(t_2) = A_1\delta_{se}(t_2)$. The variables t_1 and t_2 are not independent as they fulfill the relation $t_2 = t_1 - \triangle t$, where $\triangle t$ is the spacing between the two impulses $\delta_{se}(t)$, see Fig. 2.

In order to avoid numerical issues when applying the identified frequency domain Volterra kernel $H_{nj}(\omega_1, ..., \omega_n)$ the frequency values fulfilling the condition given in Eq. 9 are considered, where the tolerance ω_ϵ has been set to $\omega_\epsilon = 0.1$ as for the first order frequency domain Volterra kernel. At the frequency $\tilde{\omega}_n$ the equality condition is fulfilled. For frequencies $|\omega_k| > \tilde{\omega}_n$ for $k = 1, ..., n$ the frequency domain Volterra kernel $H_{nj}(\omega_1, ..., \omega_n)$ is set to zero.

$$\frac{|u_n^n(\omega)|}{max\left(|u_n^n(\omega)|\right)} \geq \omega_\epsilon \tag{9}$$

Due to the symmetry of the Volterra kernels in the time domain the Volterra kernels in the frequency domain $H_{nj}(\omega_1, ..., \omega_n)$ satisfy the conjugate symmetry property $H_{nj}(-\omega_1, ..., -\omega_n) = H_{nj}^*(\omega_1, ..., \omega_n)$ as specified by Billings et al. [31]. In order to apply the multidimensional Fourier transform the integrals in Eq. 8 have to converge and thus the Volterra kernels in the time domain $\bar{h}_{nj}(t_1, ..., t_n)$ must damp out for increasing time values. If not, multidimensional Laplace transforms must be taken into account [12, 32].

Note that for well damped dynamic systems this approach takes advantage of the small simulation times required for the response to the impulses compared to the simulation times required for a zero-mean stationary Gaussian random input. When applied to the systems under consideration in this work the well damped condition of the dynamic system implies:

- No buffeting instability occurs when applied to purely aerodynamic systems.
- No flutter / Limit Cycle Oscillation (LCO) occurs when applied to aeroelastic systems.

2.2 Nonlinear numerical solution from functional series expansion

In order to compute the nonlinear response the second order Volterra model can be applied in two numerically discretized forms:

- By applying convolution in the time domain to the output component $y_j(t)$ according to Eq. 10, where a change of each variable of integration has been used.

$$y_j(t) = \int_{-\infty}^{\infty} h_{1j}(t-\tau_1)\, u(\tau_1)\, d\tau_1 + \int_{-\infty}^{\infty}\int_{-\infty}^{\infty} h_{2j}(t-\tau_1, t-\tau_2)\, u(\tau_1)\, u(\tau_2)\, d\tau_1 d\tau_2 \quad (10)$$

The discretized version of Eq. 10 is given in Eq. 11, where $k = 1, ..., N$, with N the total number of time sample values considered. The matrix $\mathbf{T}_s = \left[\begin{array}{cc} \mathbf{I}_k & \mathbf{0} \end{array}\right]$ of size $k \times N$ selects the first k entries of the vector $\mathbf{u} = \left[\begin{array}{ccccccc} u(t_1) & \cdots & u(t_k) & \cdots & u(t_N) \end{array}\right]^T$, where $\mathbf{I}_k$ denotes the identity matrix of size k. Also, $t_1 = 0$ and $t_N = t_f$, where t_f denotes the simulation time.

$$y_j(t_k) = \frac{\triangle t}{2}\tilde{\mathbf{h}}_{1j}(t_k)\, \mathbf{T}_s(t_k)\, \mathbf{u} + \frac{\triangle t^2}{4}\left[\mathbf{T}_s(t_k)\, \mathbf{u}\right]^T \tilde{\mathbf{h}}_{2j}(t_k)\, \mathbf{T}_s(t_k)\, \mathbf{u} \quad (11)$$

A trapezoidal rule has been implemented for the convolution integrals. Matrices $\tilde{\mathbf{h}}_{1j}$ and $\tilde{\mathbf{h}}_{2j}$ are given in Appendix A.

- By computing the higher order frequency domain Volterra kernels by multidimensional Fourier transforms (the numerical implementation is the $fftn$) and recovering the response in the time domain by applying a multidimensional $ifftn$ as presented by Marzocca et al. [14], see Eq. 12 for the output component $y_j(\omega)$ of a second order Volterra system in the frequency domain.

$$\begin{aligned} y_j(\omega) &= y_{1j}(\omega) + y_{2j}(\omega) \\ &= H_{1j}(\omega)\, u(\omega) + \frac{1}{2\pi}\int_{-\infty}^{\infty} H_{2j}(\omega_1, \omega-\omega_1)\, u(\omega_1)\, u(\omega-\omega_1)\, d\omega_1 \end{aligned} \quad (12)$$

A particular aspect of the frequency domain description of the Volterra series expansion is that the output frequency range of the term $y_{2j}(\omega)$ is wider than that for $y_{1j}(\omega)$. When considering a unidimensional frequency range defined by $\omega \in [-\omega_{max}, \omega_{max}]$, the integral given in Eq. 12 for $y_{2j}(\omega)$ defines an output frequency range $\omega \in [-2\omega_{max}, 2\omega_{max}]$ as described by Billings et al. [31]. However, for the numerical application of the Volterra series, Eq. 9 is applied. With this condition typically $\tilde{\omega}_n < \tilde{\omega}_{n-1} < \omega_{max}$ and thus the new frequencies above ω_{max} are not taken into account.

The numerical discrete version of Eq. 12 is given in Eq. 13, where the output vector defined by $\mathbf{y}_j = \left[\begin{array}{ccccccc} y_j(\omega_1) & \cdots & y_j(\omega_k) & \cdots & y_j(\omega_N) \end{array}\right]^T$ contains now the complex values of the signal at the discrete frequency set, where the number of frequency samples N in the range $\omega \in [-\omega_{max}, \omega_{max}]$ is equal to the number of time samples, with $\omega_1 = -\omega_{max}$ and $\omega_N = \omega_{max}$.

The symbol $\circ$ represents the Hadamard product, that is, an element-wise multiplication. The vector $\mathbf{u} = \left[\begin{array}{cccccc} u(\omega_1) & \cdots & u(\omega_k) & \cdots & u(\omega_N) \end{array} \right]^T$ contains the frequency values of the input signal and the square matrix $\mathbf{U}$ of size N contains in each column the vector $\mathbf{u}$. The maximum possible frequency is given by the Nyquist frequency $\omega_{max} = \pi/t_s$, where t_s denotes the time step. In this work N has been selected to be odd in order to include the frequency zero. The frequency spacing is given by $\triangle\omega = 2\pi/t_f$ with t_f the total simulation time $t_f = Nt_s$. The vector $\mathbf{e}$ of length N contains one entries. The matrices and operators of Eq. 13 are defined in Appendix A.

$$\mathbf{y}_j = \tilde{\mathbf{H}}_{1j} \circ \mathbf{u} + \frac{1}{t_f} \left[\mathbf{e}^T antidiags \left(\tilde{\mathbf{H}}_{2j} \circ \mathbf{U} \circ \mathbf{U}^T \right) \mathbf{S}_1 \right]^T \tag{13}$$

In this work a nonlinear ROM for the numerical solution in the frequency domain based on Volterra or functional series is considered. It combines the continuous time impulse method from Section 2.1 for system identification with the nonlinear response computation in the frequency domain according to Eq. 13. Thus, the knowledge of the higher order frequency domain Volterra kernel in analytical form is not required and the nonlinear response to inputs defined by their frequency spectrum can be computed. As it will be seen in Section 3 this approach offers several advantages:

- The application of Eq. 13 in the frequency domain is computationally more efficient than Eq. 11 in the time domain. This is due to the fact that for the time domain solution the matrices $\mathbf{T}_s$, $\tilde{\mathbf{h}}_{1j}$ and $\tilde{\mathbf{h}}_{2j}$ in Eq. 11 have to be computed at each time step. In order to avoid the new computation of these matrices at each time step Toeplitz and doubly block Toeplitz matrices (using a rectangular instead of a trapezoidal integration rule) can be used, as described by Jain [33]. However, the doubly block Toeplitz matrices required for the second order term of the Volterra series results in a square matrix of size N^2, much bigger than the rectangular matrix of size $N \times (2N-1)$ for the frequency domain counterpart, see Appendix A.
- The computational time required by Eq. 13 is several orders of magnitude lower than that required by full-order simulations, in particular for CFD applications, see Section 3.
- It provides results even for inputs for which the full-order simulations do not converge due to high incremental values in the random Gaussian time history of the input signal.

2.2.1 Nonlinear frequency domain solution to random Gaussian excitation

For random input excitation it is usual to work with the Power Spectra Density (PSD) $\bar{\phi}_{y_j}(f)$ [1], defined as two-sided (for negative and positive frequencies) as defined by Corinthios et al. [34], $\bar{\phi}_{y_j}(f) = \lim_{t_f \to \infty} (1/t_f) \left| \mathbf{y}_j(f) \right|^2, \ \forall f \in (-\infty, \infty)$.

Assuming the input to be a zero-mean stationary Gaussian process with two-sided power spectrum $\bar{\phi}_u(f)$ the output PSD $\bar{\phi}_{y_j}(f)$ for a second order approximation by a Volterra system is given by the Mircea-Sinnreich series [35, 36], see Eq. 14. The two-sided output PSD $\phi_{y_j}(f)$ is obtained from the two-sided output PSD as $\phi_{y_j}(f) = 2\bar{\phi}_{y_j}(f), \forall f \in [0, \infty)$.

[1] In this work power signals are considered. This means that they contain an infinite energy if the regular definition of PSD for energy signals is applied, $\bar{\phi}_{y_j}(f) = \left| \mathbf{y}_j(f) \right|^2, \ \forall f \in (-\infty, \infty)$

$$\begin{aligned}\bar{\phi}_{y_j}(f) &= \bar{\phi}_u(f)\left|H_{1j}(f)+\frac{1}{2}\int_{-\infty}^{\infty}\bar{\phi}_u(f_1)\,H_{3j}(f,f_1,-f_1)\,df_1\right|^2 \\ &\quad +\frac{1}{2}\int_{-\infty}^{\infty}\bar{\phi}_u(f_1)\,\bar{\phi}_u(f-f_1)\,|H_{2j}(f_1,f-f_1)|^2\,df_1\end{aligned} \tag{14}$$

It is important to note that due to the nonlinear representation of the Volterra series the second order approximation (those which include the product of two $\bar{\phi}_u$) contains the third order frequency domain Volterra kernel H_{3j}. This means that in order to compute the proper output PSD ϕ_{y_j} there are two possibilities:

- To compute the output component y_j in the time or the frequency domain considering a representative simulation time in order to converge to the theoretical random Gaussian process of *infinite* duration.
- To consider the third order Volterra kernel H_{3j} in the frequency domain.

Both options will increase the computational time when compared to a deterministic process of finite time duration. In this work the first option is chosen as it offers a reduction in the computational time compared to that required for the identification of the third order Volterra kernel. Thus Eq. 14 is not directly used but it highlights a very important property: the output PSD $\bar{\phi}_{y_j}$ obtained by the nonlinear system approximation depends exclusively on the input PSD $\bar{\phi}_u$, i. e. the output PSD does not depend on the phase of the random Gaussian input signal.

Once the one-sided output PSD ϕ_{y_j} has been obtained the root mean square (rms) value σ_{y_j} is obtained as $\sigma_{y_j} = \left(\int_{-\infty}^{\infty}\bar{\phi}_{y_j}(f)\,df\right)^{1/2} = \left(2\int_0^{\infty}\bar{\phi}_{y_j}(f)\,df\right)^{1/2} = \left(\int_0^{\infty}\phi_{y_j}(f)\,df\right)^{1/2}$. In order to obtain a random Gaussian time history from the PSD the time signal may be considered to be generated by the superposition of an infinite number of sinusoidal components, which differ infinitesimally in frequency from one another and with a prescribed infinitesimal amplitude, being each randomly phased relative to the others. This is expressed in Eq. 15, where ω_k is the radian frequency of each component. The PSD $\Phi_u(\omega_k)$ provides the complete measure of the frequency content of the process [37]. For time domain computations it is convenient that the input signal starts at the value zero. To achieve that, a shift is applied in the time domain so that the turbulence value starts at zero, keeping its rms value, as done by Barbati et al. [38].

$$u(t) = \sum_{k=1}^{\infty}\sqrt{2\Phi_u(\omega_k)\triangle\omega}cos(\omega_k t+\psi_k), \quad \psi_k \sim 2\pi U(0,1) \tag{15}$$

In order to determine a proper time discretization both the time step t_s and the simulation time t_f have to been specified by imposing a convergence to the theoretical Gaussian distribution. This is done in two steps, assuming that the input PSD ϕ_u and its rms value σ_u are known:

1. First the maximum frequency f_{max} to be considered is determined by imposing a convergence in the rms of the input signal σ_u,

$$\left|\left(\int_0^{f_{max}}\phi_u(f)\,df\right)^{1/2}-\sigma_u\right|/\sigma_u \leq \sigma_\epsilon \tag{16}$$

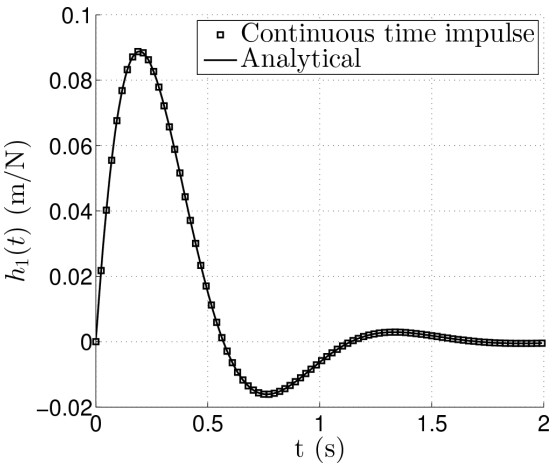

Figure 3: First order kernel (continuous time impulse method and analytical) for nonlinear oscillator.

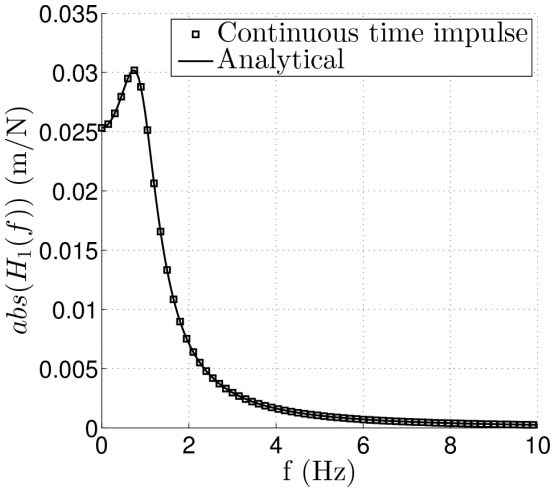

Figure 4: First order transfer function (continuous time impulse method and analytical) for nonlinear oscillator (magnitude).

A frequency spacing $\triangle f$ depending on the particular input PSD ϕ_u is defined for the numerical integration. Once the frequency spacing is defined the maximum frequency f_{max} is increased until the condition defined by Eq. 16 is reached. The tolerance value has been set to $\sigma_\epsilon = 0.01$. The maximum or Nyquist frequency f_{max} specifies the required time step, $t_s = 1/2f_{max}$.

2. Second the simulation time t_f is increased until convergence in the rms of the input signal σ_u is achieved,

$$\left| \left(\frac{1}{t_f} \int_0^{t_f} |u(t)|^2 \, dt \right)^{1/2} - \sigma_u \right| / \sigma_u \leq \sigma_\epsilon \tag{17}$$

In Eq. 17 the Parseval theorem has been applied and the factor $1/t_f$ appears for power signals. The signal $u(t)$ is computed in the time domain considering a finite summation in Eq. 15 up to $\omega_{max} = 2\pi f_{max}$, where the maximum frequency f_{max} has been obtained in step 1. As for step 1 the tolerance is set to $\sigma_\epsilon = 0.01$. The time step t_s from step 1 together with the simulation time t_f from step 2 specify the time discretization required for the second order Volterra system representation for a random Gaussian input.

2.3 One degree of freedom nonlinear system

In this Section a one degree of freedom nonlinear oscillator as considered by Prazenica [10] is analyzed. The system output $y(t)$ satisfies the nonlinear differential equation given in Eq. 18, where $u(t)$ denotes the system input.

$$m\ddot{y}(t) + c\dot{y}(t) + k_1 y(t) + k_2 y^2(t) = u(t) \tag{18}$$

The system parameters are $m = 1$ (kg), $c = 6$ (N m/s), $k_1 = 4\pi^2$ (N/m) and $k_2 = 4\pi^2$ (N/m^2).

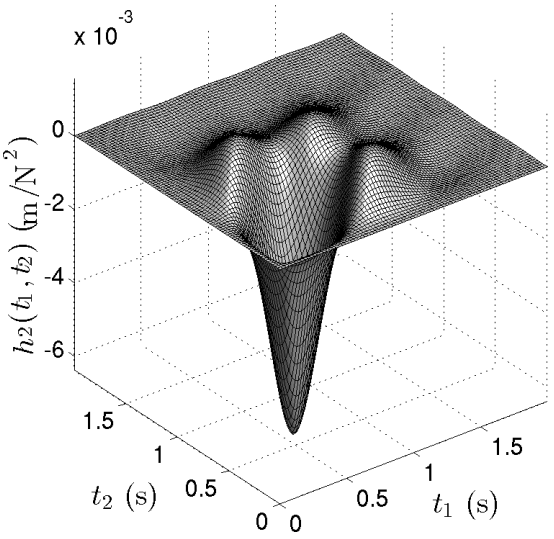

Figure 5: Second order Volterra kernel (analytical) for nonlinear oscillator.

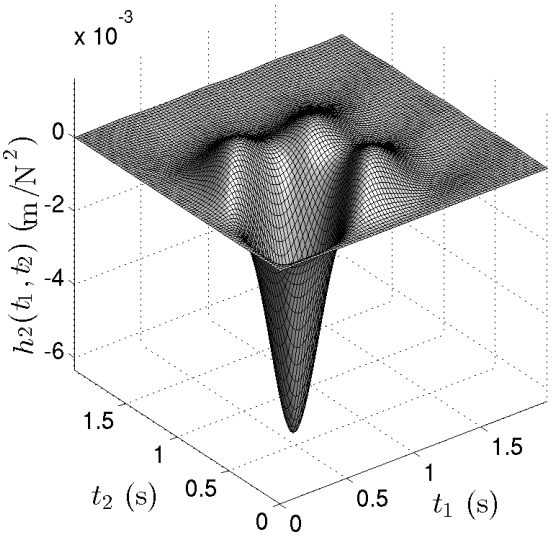

Figure 6: Second order Volterra kernel (continuous time impulse method) for nonlinear oscillator.

First the Volterra kernels of first and second order are identified with the continuous time impulse method presented in Section 2.1. For the nonlinear oscillator the kernels in the frequency domain can be computed analytically with the harmonic probing method [15] and may be used for validation purposes, see Appendix B. Note that the higher order frequency domain Volterra kernels are independent of the signal input. The analytical version of the kernels in the time domain correspond to the multidimensional inverse Fourier transform of the analytical higher frequency domain Volterra kernels. Fig. 3 and 4 show a comparison of the first Volterra kernel obtained with the continuous time impulse method and the analytical functions in the time domain and frequency domain. As it can be seen, the agreement is excellent. Fig. 5 and 6 show the second Volterra kernel in the time domain obtained in analytical form and with the continuous time impulse method, respectively. Again, a very good agreement with the analytical form is observed.

Several tests have been conducted for the nonlinear oscillator system by imposing several inputs defined by Prazenica [10], showing a very good agreement between the second order Volterra series approximation and the direct nonlinear numerical simulation. These tests are not shown in this paper but have been used for validation. Next a random Gaussian input with von Kármán PSD Φ_u defined in Eq. 22 of Section 3.2 is considered after setting $\Phi_{pk} = \Phi_u$ and $\sigma_w = \sigma_u$. The two conditions given in Eq. 16 and 17 together with a frequency spacing $\triangle f = 0.46U_\infty/4\pi L$ as recommended by Hoblit [39] (U_∞ is the gust translational speed and L the scale of the turbulence, see Section 3.2) a time step value of $t_s = 0.033$ (s) and a simulation time of $t_f = 236$ (s) are obtained. These values ensure that the rms value σ_u obtained from the time histories are representative of the *infinite* duration Gaussian process. Fig. 7 shows the output $y(t)$ for a random Gaussian input with rms value of $\sigma_u = 1.3333$ (N). The first order and second order response obtained with the frequency domain Volterra kernel according to Eq. 13 are compared to the full-order simulation. The zoomed region shows the appearance of nonlinearities and its proper prediction by the second order Volterra series. Fig. 8 shows the dependency of the output rms σ_y as function of the input rms σ_u. The zoomed region shows that the Volterra second order expansion predicts the proper trend when compared to the full order simulation. There are two

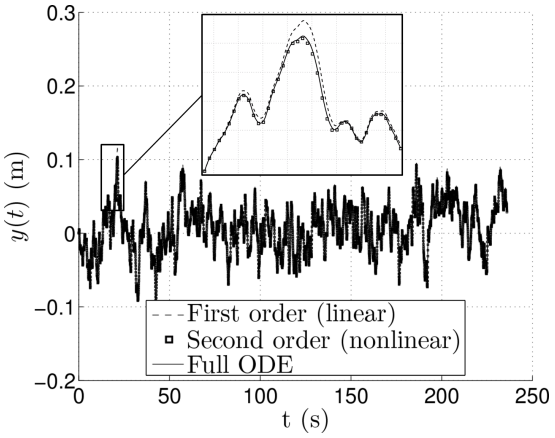

Figure 7: Output to Gaussian random signal computed with the frequency domain Volterra kernel for nonlinear oscillator. The input rms is set to $\sigma_u = 1.3333$.

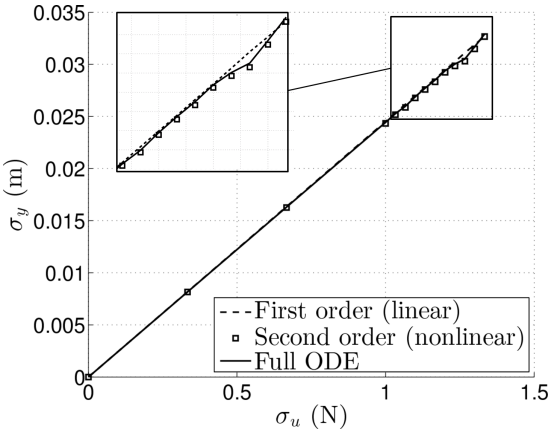

Figure 8: Output rms σ_y as function of input rms σ_u.

additional limitations that have to be considered:

- The second order Volterra expansion is valid up to a particular rms input σ_u value, above which a higher order approximation is required. For this system the second order Volterra expansion shows a satisfactory trend in the $\sigma_y\left(\sigma_u\right)$ curve up to values of $\sigma_u \approx 2$ (N).
- The full ODE simulation shows convergence problems for increasing σ_u values. For this system the numerical integration scheme does not converge above $\sigma_u \approx 5.5$ (N).

3 NONLINEAR FREQUENCY DOMAIN AERODYNAMIC MODEL

In this work the structural model is considered to be rigid and does not undertake any motion. The only aerodynamic input degree of freedom considered is the nondimensional (through U_∞) vertical gust velocity $w_d(t)$ at a reference point, fixed at the aircraft nose. The system output is the vector of length N_h (with N_h the number of considered generalized coordinates) of Generalized Aerodynamic Forces (GAF), which are obtained after projection of the acting aerodynamic loads $\mathbf{P}_g$ into the structural modes contained in the matrix $\boldsymbol{\phi}_{gh}$, $\mathbf{GAF}\left(M_\infty, k, \alpha_s\right) = \boldsymbol{\phi}_{gh}^T \mathbf{P}_g\left(M_\infty, k, \alpha_s\right)$, where M_∞ is the freestream Mach number, k the reduced frequency and α_s the steady angle of attack. The reduced frequency k is defined as $k = 2\pi f L_{ref}/U_\infty$, where L_{ref} is a reference length, typically the half of the Mean Aerodynamic Chord (MAC), and U_∞ the freestream velocity.

In order to account for aerodynamic nonlinearities in the frequency domain, a Volterra or functional series expansion is considered, see Eq. 19, based on Eq. 4.

$$\begin{aligned} \mathbf{GAF}\left(M_\infty, k, \alpha_s\right) &= \mathbf{Q}_{hd1}\left(M_\infty, k, \alpha_s\right) w_d\left(k\right) \\ &+ \frac{U_\infty}{2\pi L_{ref}} \int_{-\infty}^{\infty} \mathbf{Q}_{hd2}\left(M_\infty, k_1, k-k_1, \alpha_s\right) w_d\left(k_1\right) w_d\left(k-k_1\right) dk_1 \end{aligned} \tag{19}$$

The first term $\mathbf{Q}_{hd1}$ in Eq. 19 represents the linear(ized) part. For a complete aeroelastic model including aircraft free flexible motion the aeroelastic ROM presented by Quero [4] can be used

Property	Wing	Horizontal Tail Plane	Vertical Tail Plane
Span (m)	57.80	18.00	11.75
Aspect ratio	8.7	4.1	1.7
Root chord (m)	13.02	6.49	10.2
Sweep angle at leading edge (deg)	35.9	47.7	41.4
Taper ratio	0.591	0.354	0.317

Table 1: Geometrical properties.

Figure 9: Inviscid wing empennage configuration. Steady pressure coefficient distribution at $M_\infty = 0.84$ and $\alpha_s = 2$ (deg).

for its determination. The matrices $\mathbf{Q}_{hd1}$ and $\mathbf{Q}_{hd2}$ are of size $(N_h \times 1)$, as w_d refers to the nondimensional disturbance velocity at the aircraft nose. In this work the matrices $\mathbf{Q}_{hd1}$ and $\mathbf{Q}_{hd2}$ are obtained with the continuous time impulse method described in Section 2.1.

Now the continuous time impulse method is applied to a wing empennage configuration. The geometrical properties are shown in Table 1. The reference length for the reduced frequency is $L_{ref} = 4.5$ (m). The Mach number is set to $M_\infty = 0.84$ and the initial (steady) angle of attack to $\alpha_s = 2$ (deg), see Fig. 9, which shows the presence of a shock wave over the upper wing surface. Once the frequency domain Volterra kernels have been identified, discrete *1-cos* gust and continuous turbulence encounters are considered.

When considering the gust as input the impulse shape δ_{sc} is considered to be of *1-cos* shape rather than the exponential form of Eq. 5, see Eq. 20, where L_g denotes the gust length. Note that the gust penetration effect is included automatically by convecting the gust profile with a translational speed U_∞. The gust reduced frequency is given by $k_g = 2\pi L_{ref}/L_g$ and is inversely proportional to the gust length L_g.

$$\delta_{sc}(t) = \begin{cases} \frac{1}{2U_\infty}\left[1 - cos\left(\frac{1}{L_g}\left(2\pi U_\infty t\right)\right)\right], & 0 \leq t \leq \frac{L_g}{U_\infty}, \\ 0, & else \end{cases} \tag{20}$$

The corresponding nondimensional gust input for the first and second order Volterra kernel identification w_{d1} and w_{d2} are given in Eq. 21 respectively. The values $A_1 = \pi/180$ and $A_2 = 4\pi/180$ have been chosen, which represent a $1 - cos$ pulse of equivalent angle of attack $\alpha_{eq} = tan\left(A_n/U_\infty\right)$ of 1 and 4 (deg) respectively. Fig. 10 shows the corresponding dimensional gust field at the initial time $t = 0$. For the second order kernel identification the corresponding gust field for a value of $\triangle t = 0.26$ (s) is shown.

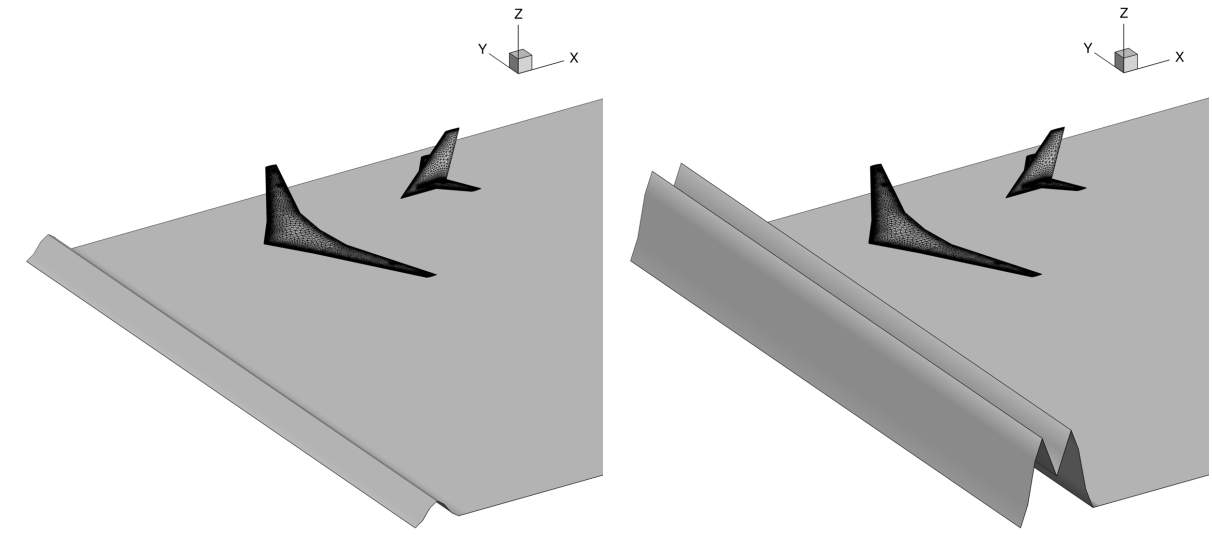

(a) Input $U_\infty w_{d1}(t)$ for first order kernel identification. (b) Input $U_\infty w_{d2}(t)$ for second order kernel identification, $\triangle t = 0.026$ (s).

Figure 10: Gust field input at initial time $t = 0$ for Volterra kernel identification.

$$w_{d1}(t) = A_1 \delta_{sc}(t), \quad w_{d2}(t) = A_2 \left[\delta_{sc}(t) + \delta_{sc}(t - \triangle t)\right] \tag{21}$$

In order to identify the first order $\mathbf{Q}_{hd1}$ and second order $\mathbf{Q}_{hd2}$ frequency domain Volterra kernels, a damped aerodynamic system is required, see Section 2.1. In the case the numerical solution to the gust impulse functions does not tend to an exact zero value, a *detrend* scheme is implemented for the first order Volterra kernel in the time domain. This scheme ensures that the output signal starts and ends at zero avoiding numerical noise when applying the Fourier transform by substracting the linear trend between the initial and end values of the numerical solution, as discussed by Teufel et al. [40]. For higher order Volterra kernels the possible non-zero value $\lim_{\triangle t \to \infty} \mathbf{Q}_{hd2}(t_1, t_2)$ is substracted from $\mathbf{Q}_{hd2}(t_1, t_2)$. For the practical implementation the time lag $\triangle t$ is usually smaller than the simulation time, $max(\triangle t) = \triangle t_f < t_f$, and thus the value $\mathbf{Q}_{hd2}(t_1, t_1 - \triangle t_f)$ is substracted from $\mathbf{Q}_{hd2}(t_1, t_2)$. Fig. 11 shows the second order Volterra kernel in the time domain and in the frequency domain from the atmospheric disturbance $w_d(t)$ to the GAF projected into the pitch mode, computed according to the continuous impulse method of Section 2.1 and after a numerical bidimensional Fourier transform for the frequency domain counterpart. The condition defined by Eq. 9 has also been applied after setting $u_2 = w_{d2}$.

3.1 Discrete gust

In this Section a *1-cos* discrete gust of amplitude $\alpha_{eq} = 3.62$ (deg) and half gust length $H = L_g/2 = 350$ (ft), the longest according to the regulations [41], equivalent to a gust reduced frequency $k_g = 0.13$, is considered. Note that this gust amplitude lies in between the gust amplitudes of $\alpha_{eq} = 1$ (deg) and $\alpha_{eq} = 4$ (deg) used for the Volterra kernels identification. The nonlinear ROM output is computed in the frequency domain as described in Eq. 13. Fig. 12 shows a comparison between the linear(ized) or first order Volterra, the second order Volterra series expansion and the full-order CFD computation. The peaks predicted by the first order

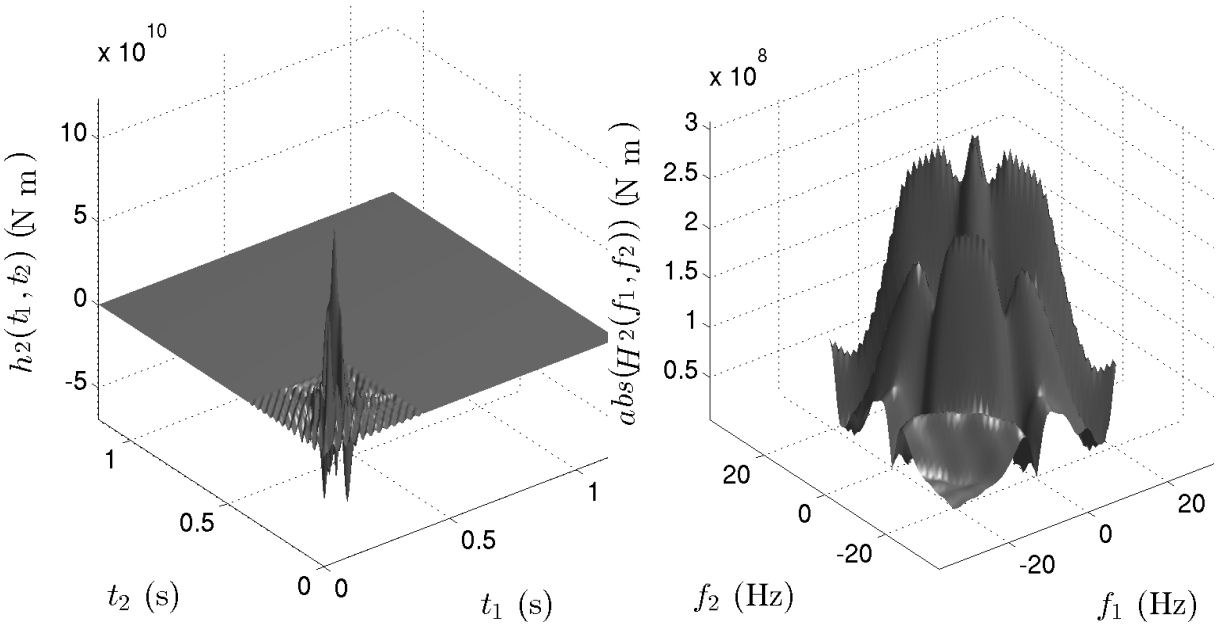

(a) Second order Volterra kernel.

(b) Second order frequency domain Volterra kernel.

Figure 11: Second order Volterra kernel from atmospheric disturbance w_d to generalized aerodynamic pitch moment. $M_\infty = 0.84$ and $\alpha_s = 2$ (deg).

Volterra series expansion are higher than those predicted by CFD. The second order Volterra series expansion notably improves the predicted linear(ized) results, reducing the maximum relative peak deviation from 7.7 % for the first order Volterra expansion down to 1.9 % for the generalized aerodynamic vertical force and from 8.5 % down to 4.1 % for the generalized aerodynamic pitch moment. Regarding the computational time, the nonlinear ROM presents a reduction on the computational time of four orders of magnitude compared to the full-order CFD simulation for the discrete gust case. The computational case for this example has been 5 (s) for the nonlinear ROM (carried out on an Intel Xeon X5690 processor at 3.47 GHz and cache size of 12 MB) and 10500 (s) for the CFD computation (carried out on an Intel Xeon X5650 processor with 32 cores at 2.67 GHz and 12 MB).

3.2 Continuous turbulence

In this Section a random Gaussian input is considered as atmospheric disturbance. Two different functions for describing the gust PSD in continuous turbulence have been commonly used, the Dryden and the von Kármán spectrum, provided in Eq. 22 as $\Phi_{pk}(\omega)$ (one-sided) depending on the parameters p and k, where σ_w represents the rms value of the turbulence [42]. For Dryden $p = 1/2$ and $k = 1$, whereas for von Kármán $p = 1/3$ and $k = 1.339$. Due to the better fit to atmospheric data, the von Kármán spectrum is used here. The scale of turbulence L is set to 2500 (ft) as proposed by Hoblit [39].

$$\Phi_{pk}(\omega) = \sigma_w^2 f_{pk}(\omega) = \sigma_w^2 \left(\frac{L}{\pi U_\infty}\right) \frac{1 + 2(p+1)(kL\omega/U_\infty)^2}{\left[1 + (kL\omega/U_\infty)^2\right]^{p+3/2}},\ \omega \geq 0 \tag{22}$$

Fig. 13 shows the relative percent deviation of the GAF rms (projected into the heave and pitch modes) obtained by second order Volterra series expansion σ_{GAF2} with respect to the rms value

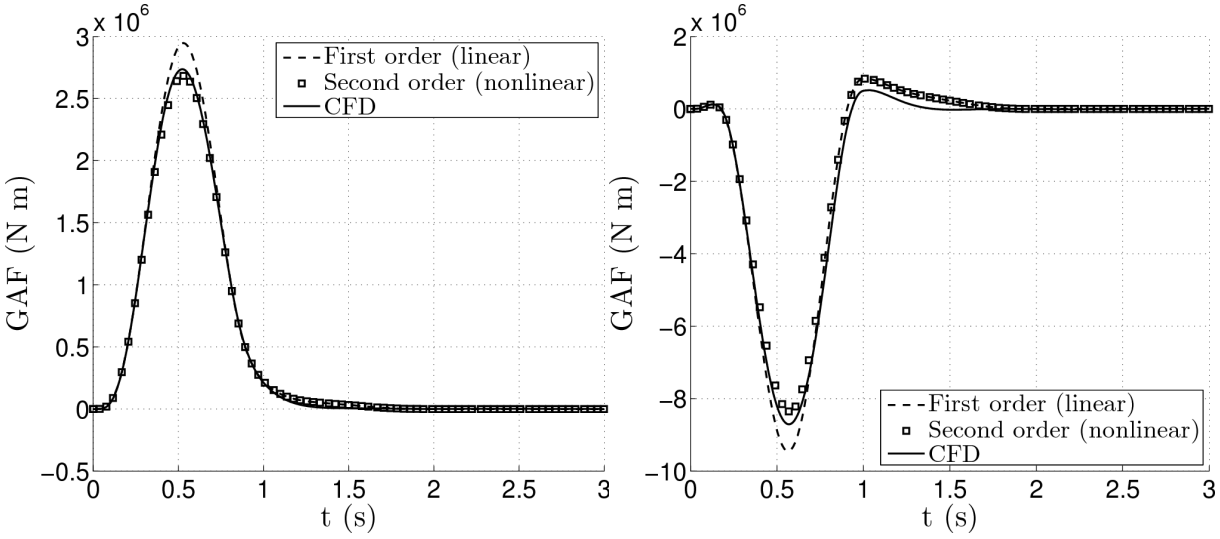

(a) Heave mode.

(b) Pitch mode.

Figure 12: GAF for gust input $\alpha_{eq} = 3.62$ (deg) and $k_g = 0.13$. $M_\infty = 0.84$ and $\alpha_s = 2$ (deg).

obtained by the first order Volterra series expansion or linear(ized) solution σ_{GAF1}, computed as $100\left(\sigma_{GAF2} - \sigma_{GAF1}\right) / \left|\sigma_{GAF1}\right|$, versus the turbulence rms σ_w up to a maximum value of $\sigma_w = 12$ (m/s). Similar to the nonlinear oscillator of Section 2.3 a small reduction of the GAF rms σ_{GAF} is predicted by the nonlinear Volterra series expansion of second order. Note that an additional convergence study adding the third order Volterra kernel would reveal up to which value of the turbulence rms σ_w the second order expansion is appropriate, but it has not been further investigated. Additionally a polynomial quadratic fit for the curves in Fig. 13 is shown. As it can be observed the quadratic fit reproduces very well the predicted nonlinear deviation behaviour of the GAF rms values. The computational time of the nonlinear ROM for this case has been of 650 (s), higher than for the discrete gust, due to the small frequency spacing $\triangle f = 0.004237$ (Hz) produced by the long simulation time $t_f = 236$ (s) imposed by Eq. 17 and obtained in Section 2.3. In the case of continuous turbulence no reference data from CFD could be generated due to the following issues:

- The CFD simulation does not converge for turbulence rms values higher than $\sigma_w \approx 2$ (m/s) due to the high incremental values experience in the turbulence disturbance $w_d\left(t\right)$ in one time step.
- Very long simulation times are required in order to reproduce the Gaussian random distribution. By taking into account the computational time required by CFD for the discrete gust in Section 3.1 this would mean an approximately computational time of $4.956 \cdot 10^5$ (s) if the solution were to converge. This would represent an approximate reduction in the computational time of up to four orders of magnitude, similar to that obtained for the discrete gust case.

According to the quadratic fit shown in Fig. 13 the nonlinear GAF rms vector of length N_h as predicted by the second order Volterra series expansion $\boldsymbol{\sigma}_{GAF2}$ can thus be expressed as function of the turbulence rms σ_w with a cubic polynomial approximation, see Eq. 23, where $\boldsymbol{\sigma}_{GAF1}$ corresponding to the first order approximation of the Volterra or functional series is obtained by setting $\boldsymbol{\alpha}_1 = \boldsymbol{\alpha}_2 = \mathbf{0}$.

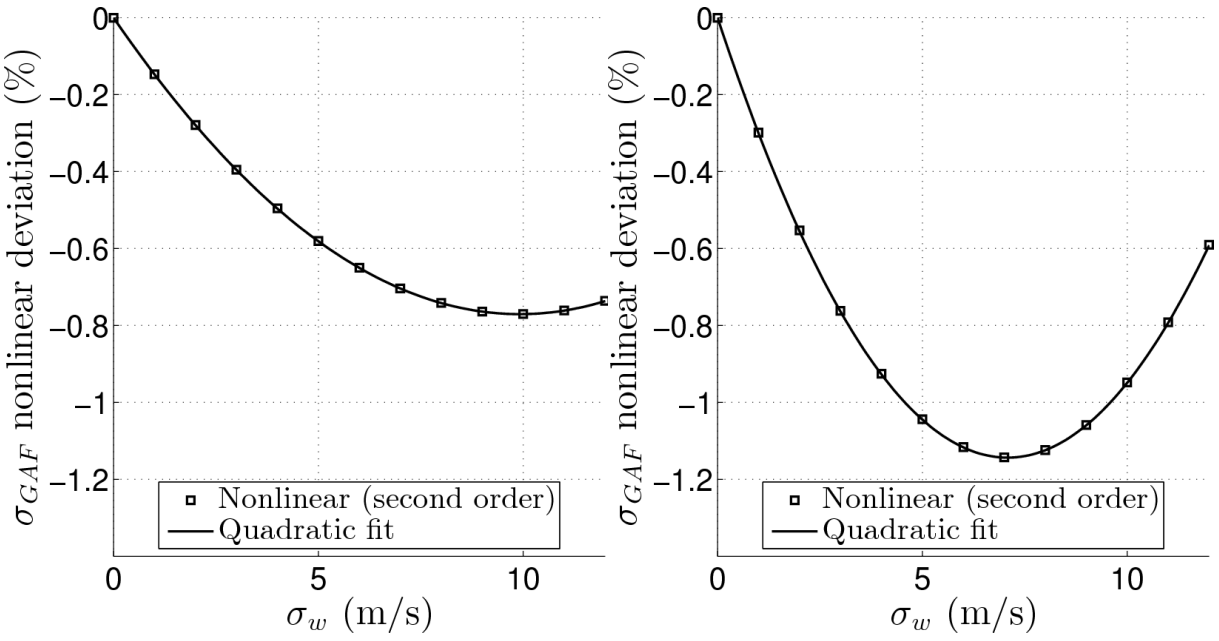

(a) Heave mode.

(b) Pitch mode.

Figure 13: GAF rms σ_{GAF} deviation of second order with respect to first order Volterra series expansion as function of the turbulence rms σ_w. $M_\infty = 0.84$ and $\alpha_s = 2$ (deg).

$$\boldsymbol{\sigma}_{GAF2} = \sigma_w \left[\int_0^\infty \left| \mathbf{Q}_{hd1}(\omega) \right|^2 f_{pk}(\omega) \right]^{1/2} \left(1 + \boldsymbol{\alpha}_1 \sigma_w + \boldsymbol{\alpha}_2 \sigma_w^2 \right) \tag{23}$$

For the case considered the vectors $\boldsymbol{\alpha}_1$ and $\boldsymbol{\alpha}_2$ of length $N_h = 2$ corresponding to the heave and pitch GAF are

$$\boldsymbol{\alpha}_1 = \begin{bmatrix} -1.5541 \\ -3.2305 \end{bmatrix} 10^{-3} \ \left(1/\left(m/s\right)\right), \ \boldsymbol{\alpha}_2 = \begin{bmatrix} 0.7835 \\ 2.2811 \end{bmatrix} 10^{-4} \ \left(1/\left(m/s\right)^2\right)$$

4 CONCLUSION

To the author's knowledge the Volterra series expansion had not yet been applied to the nonlinear aerodynamic contribution due to turbulence encounters in the frequency domain. In this work a novel nonlinear ROM based on the identification of the Volterra kernels with continuous time impulses and its numerical application in the frequency domain for the nonlinear aerodynamic response prediction to gust and continuous turbulence encounters has been presented. The method notably improves the linear(ized) prediction. A nonlinear dependency of the GAF rms as function of the turbulence rms has been obtained for Gaussian continuous turbulence encounter. This relation is only dependent on the turbulence frequency content and independent of the phase content.

The presented nonlinear ROM provides several advantages:

- The nonlinear system identification follows from the application of continuous (with high frequency content) and not discrete input impulses, which improves the convergence of the CFD simulations required for the Volterra kernel identification.

- The nonlinear response can be computed by the present ROM much faster than by a full-order nonlinear simulation, provided the Volterra kernels have been identified. Additionally the frequency domain implementation requires less computational effort than the time domain implementation.
- It is applicable to cases for which the full-order nonlinear simulation does not converge. Massive CFD convergence problems have been observed for continuous turbulence profiles with a root mean square (rms) value higher than approximately 2 (m/s). This seems to be a serious limitation, specially when turbulence encounters specified by the regulations contain rms values higher than 10 (m/s).

As continuation of this work several extensions are proposed:

- Consideration of multi-input systems for several aerodynamic excitations acting simultaneously. This implies the consideration of cross Volterra kernels [15].
- Development of a nonlinear aeroelastic solver in the frequency domain by coupling the nonlinear ROM with the structural model. In order to achieve this the multi-input formulation has to be implemented, as the effects of both the atmospheric disturbance and the aircraft motion have to be considered.
- Application to optimization problems in order to find the worst gust case scenario as an extension of the linear Matched Filter Theory following the idea of Scott et al. [43].

APPENDIX A: MATRICES IN THE NUMERICAL IMPLEMENTATION OF VOLTERRA OR FUNCTIONAL SERIES EXPANSION

The matrix $\tilde{\mathbf{h}}_{1j}$ of size $1 \times k$ in Eq. 11 is given by:

$$\tilde{\mathbf{h}}_{1j}\left(t_k\right) = \left[\begin{array}{ccccccc} h_{1j}\left(t_k\right) & 2h_{1j}\left(t_{k-1}\right) & \cdots & 2h_{1j}\left(t_i\right) & \cdots & 2h_{1j}\left(t_2\right) & h_{1j}\left(t_1\right) \end{array}\right]$$

, where $i = 1, ..., k$. The square matrix $\tilde{\mathbf{h}}_{2j}$ of size k is:

$$\tilde{\mathbf{h}}_{2j}\left(t_k\right) = \left[\begin{array}{cccccc} h_{2j}\left(t_k, t_k\right) & 2h_{2j}\left(t_{k-1}, t_k\right) & \cdots & \cdots & 2h_{2j}\left(t_2, t_k\right) & h_{2j}\left(t_1, t_k\right) \\ 2h_{2j}\left(t_k, t_{k-1}\right) & 4h_{2j}\left(t_{k-1}, t_{k-1}\right) & & & 4h_{2j}\left(t_2, t_{k-1}\right) & 2h_{2j}\left(t_1, t_{k-1}\right) \\ \vdots & \vdots & \ddots & & \vdots & \vdots \\ 2h_{2j}\left(t_k, t_i\right) & 4h_{2j}\left(t_{k-1}, t_i\right) & & \ddots & 4h_{2j}\left(t_2, t_i\right) & 2h_{2j}\left(t_1, t_i\right) \\ \vdots & \vdots & & & \vdots & \vdots \\ 2h_{2j}\left(t_k, t_2\right) & 4h_{2j}\left(t_{k-1}, t_2\right) & & & 4h_{2j}\left(t_2, t_2\right) & 2h_{2j}\left(t_1, t_2\right) \\ h_{2j}\left(t_k, t_1\right) & 2h_{2j}\left(t_{k-1}, t_1\right) & \cdots & \cdots & 2h_{2j}\left(t_2, t_1\right) & h_{2j}\left(t_1, t_1\right) \end{array}\right]$$

In Eq. 13 the discrete versions of the frequency domain Volterra kernel obtained by uni- and bidimensional Fourier transforms for the output component y_j have been used,

$$\tilde{\mathbf{H}}_{1j} = \left[\begin{array}{ccc} H_{1j}\left(\omega_1\right) & \cdots & H_{1j}\left(\omega_N\right) \end{array}\right]^T$$

$$\tilde{\mathbf{H}}_{2j} = \begin{bmatrix} H_{2j}(\omega_1,\omega_1) & \cdots & H_{2j}(\omega_1,\omega_k) & \cdots & H_{2j}(\omega_1,\omega_N) \\ \vdots & & \vdots & & \vdots \\ H_{2j}(\omega_k,\omega_1) & & H_{2j}(\omega_k,\omega_k) & & H_{2j}(\omega_k,\omega_N) \\ \vdots & & \vdots & & \vdots \\ H_{2j}(\omega_N,\omega_1) & \cdots & H_{2j}(\omega_N,\omega_k) & \cdots & H_{2j}(\omega_N,\omega_N) \end{bmatrix}$$

, where the matrix $\tilde{\mathbf{H}}_{2j}$ is symmetric. The operator $antidiags$ takes the proper anti- or secondary diagonals of a square matrix. Applying the operator $antidiags$ to a square matrix $\mathbf{A}$ of size N results in a rectangular matrix of size $N \times (2N-1)$, which is responsible for the extension of the frequency interval to $\omega \in [-2\omega_{max}, 2\omega_{max}]$,

$$antidiags(\mathbf{A}) = antidiags\left(\begin{bmatrix} A_{11} & A_{12} & \cdots & A_{1k} & \cdots & A_{1,N-1} & A_{1N} \\ A_{21} & \vdots & & \vdots & & A_{2,N-1} & A_{2N} \\ \vdots & \vdots & & \vdots & & \vdots & \vdots \\ A_{k1} & \vdots & & A_{kk} & & \vdots & A_{kN} \\ \vdots & \vdots & & \vdots & & \vdots & \vdots \\ A_{N-1,N} & A_{N-1,2} & & \vdots & & \vdots & A_{N-1,N} \\ A_{N,1} & A_{N,2} & \cdots & A_{Nk} & \cdots & A_{N,N-1} & A_{N,N} \end{bmatrix}\right)$$

$$= \begin{bmatrix} A_{11} & A_{21} & \cdots & A_{k1} & \cdots & A_{N-1,1} & A_{N,1} & A_{N,2} & \cdots & A_{Nk} & \cdots & A_{N,N-1} & A_{NN} \\ 0 & A_{12} & & \vdots & & \vdots & A_{N-1,2} & \vdots & & \vdots & & A_{N-1,N} & 0 \\ \vdots & 0 & & A_{1k} & & \vdots & \vdots & \vdots & & A_{kN} & & 0 & \vdots \\ \vdots & \vdots & & 0 & & \vdots & \vdots & \vdots & & 0 & & \vdots & \vdots \\ \vdots & \vdots & & \vdots & & \vdots & \vdots & \vdots & & \vdots & & \vdots & \vdots \\ \vdots & \vdots & & \vdots & & A_{1,N-1} & A_{2,N-1} & A_{2,N} & & \vdots & & \vdots & \vdots \\ 0 & 0 & 0 & 0 & 0 & 0 & A_{1,N} & 0 & 0 & 0 & 0 & 0 & 0 \end{bmatrix}$$

The sum over the complex elements of the matrix $antidiags\left(\tilde{\mathbf{H}}_{2j} \circ \mathbf{U} \circ \mathbf{U}^T\right)$ is carried out by the row vector $\mathbf{e}^T$ with one entries of length N in Eq. 13. The matrix $\mathbf{S}_1 = \begin{bmatrix} \mathbf{0}^T & \mathbf{I}_N & \mathbf{0}^T \end{bmatrix}^T$ of size $(2N-1) \times N$ selects the frequency range $\omega \in [-\omega_{max}, \omega_{max}]$, where $\mathbf{I}_N$ is the identity matrix of size N. The zero submatrices are of size $(N-1)/2 \times N$.

APPENDIX B: HIGHER ORDER FREQUENCY DOMAIN VOLTERRA KERNELS FOR NONLINEAR OSCILLATOR

The higher order frequency domain Volterra kernels for the nonlinear oscillator can be computed by means of the harmonic probing technique as described by Worden et al. [15]. For the nonlinear oscillator defined in Eq. 18 they are provided up to the third order in Eq. 24, 25 and 26.

$$H_1(\omega) = \frac{1}{-m\omega^2 + ic\omega + k_1} \tag{24}$$

$$H_2(\omega_1,\omega_2) = -k_2 H_1(\omega_1) H_1(\omega_2) H_1(\omega_1+\omega_2) \tag{25}$$

$$\begin{aligned} H_3(\omega_1,\omega_2,\omega_3) &= -\frac{2k_2}{3} H_1(\omega_1+\omega_2+\omega_3) \\ &\quad [H_1(\omega_1) H_2(\omega_2,\omega_3) + H_1(\omega_2) H_2(\omega_3,\omega_1) + H_1(\omega_3) H_2(\omega_1,\omega_2)] \end{aligned} \tag{26}$$

5 REFERENCES

[1] Albano, E., and Roden, W.P., *A doublet-lattice method for calculating lift distributions on oscillating surfaces in subsonic flows*, AIAA Journal, Vol. 7, No. 2, 1969.

[2] Silva, W., *Recent Enhancements to the Development of CFD-Based Aeroelastic Reduced-Order Models*, 48th AIAA/ASME/ASCE/AHS/ASC Structures, Structural Dynamics, and Materials Conference, Honolulu, Hawaii (USA), 2007.

[3] Ripepi, M., *Model Order Reduction for Computational Aeroelasticity*, Doctoral Dissertation Politecnico di Milano, 2014.

[4] Quero, D., *An Aeroelastic Reduced Order Model for Dynamic Response Prediction to Gust Encounters*, Doctoral Dissertation Technical University of Berlin, 2017.

[5] Silva, W. A., *Reduced Order Models based on Linear and Nonlinear Aerodynamic Impulse Responses*, 40th Structures, Structural Dynamics & Materials Conference, St. Louis, Missouri (USA), 1999.

[6] Boyd, S., and Chua, L., *Fading Memory and the Problem of Approximating Nonlinear Operators with Volterra Series*, IEEE Transactions on Circuits and Systems, Vol. 32, No. 11, 1985.

[7] Boyd, S., Chua, L., and Desoer, C., *Analytical Foundations of Volterra Series,* IMA Journal of Mathematical Control and Information, Vol. 1, No. 3, 1984.

[8] Li, L., and Billings, S., *Discrete time subharmonic modelling and analysis*, International Journal of Control, Vol. 78, No 16, 2005.

[9] Ku, Y., and Wolf, A., *Volterra-Wiener functionals for the analysis of nonlinear systems*, Journal of the Franklin Institute, Vol. 281, No. 1, 1966.

[10] Prazenica, R., *Wavelet-based Volterra series representations of nonlinear dynamical systems*, Dissertation, University of Florida, 2002.

[11] Lang, Z. Q., and Billings, S. A., *Output frequency characteristics of nonlinear systems*, International Journal of Control, Vol. 64, No. 6, 1996.

[12] Debnath, J., and Debnath, N. C., *Theorems on Association of Variables in Multidimensional Laplace Transforms*, International J. Math. & Math. Sci., Vol. 12, No. 2, 1989.

[13] Silva, W., *Identification of nonlinear aeroelastic systems based on the Volterra theory: progress and opportunities*, Nonlinear Dynamics, Vol. 39, No. 1, 2005.

[14] Marzocca, P., Librescu, L., and Silva, W., *Aeroelastic response of nonlinear wing sections using a functional series technique*, AIAA Journal, Vol. 40, No. 5, 2002.

[15] Worden, K., Manson, G., and Tomlinson, G., *A harmonic probing algorithm for the multi-input Volterra series*, Journal of Sound and Vibration, Vol. 201, No. 1, 1997.

[16] Balajewicz, M., Nitzsche, F., and Feszty, D., *Application of multi-input Volterra theory to nonlinear multi-degree-of-freedom aerodynamic systems*, AIAA Journal, Vol. 48, No 1, 2010.

[17] Khawar, J., Zhigang, W., and Chao, Y., *Volterra kernel identification of MIMO aeroelastic system through multiresolution and multiwavelets*, Computational Mechanics, Vol. 49, No. 4, 2012.

[18] Lee, Y. W., and Schetzen, M., *Measuring of the Wiener kernels of a non-linear systems by cross-correlation*, International Journal of Control, Vol. 2, No. 3, 1965.

[19] Wiener, N., *Nonlinear Problems in Random Theory*, M.I.T. Press, Cambridge, MA, 1958.

[20] Kurdila, A., Prazenica, R., Rediniotis. O., and Srganac, T., *Multiresolution methods for reduced-order models for dynamical systems*, Journal of Guidance, Control, and Dynamics, Vol. 24, No. 2, 2001.

[21] Marmarelis, V. Z., *Identification of nonlinear biological systems using Laguerre expansions of kernels*, Annals of Biomedical Engineering, Vol. 21, No. 6, 1993.

[22] Reisenthel, P., *Prediction of unsteady aerodynamic forces via nonlinear kernel identification*, IFASD, Williamsburg, Virginia (USA), 1999.

[23] Wray, J., and Green, G., *Calculation of the Volterra kernels of non-linear dynamic systems using an artificial neural network*, Biological Cybernetics, Vol. 71, No. 3, 1994.

[24] Silva, W., *Application of nonlinear systems theory to transonic unsteady aerodynamic responses*, Journal of Aircraft, Vol. 30, No. 5, 1993.

[25] Raveh, D., *Reduced-order models for nonlinear unsteady aerodynamics*, AIAA Journal, Vol. 39, No. 8, 2001.

[26] Schetzen, M., *Measurement of the Kernels of a Non-linear System of Finite Order*, International Journal of Control, Vol. 1, No. 3, 1965.

[27] Silva, W. A, *Identification of linear and nonlinear aerodynamic impulse responses using digital filter techniques*, 22nd Atmospheric Flight Mechanics Conference, New Orleans, Louisiana (USA), 1997.

[28] Milanese, A., and Marzocca, P., *Volterra Kernels Identification Using Continuous Time Impulses Applied to Nonlinear Aeroelastic Problems*, 50th AIAA/ASME/ASCE/AHS/ASC Structures, Structural Dynamics, and Materials Conference, Palm Springs, California (USA), 2009.

[29] Marques, A. N., and Azevedo, J. L. F., *Numerical Calculation of Impulsive and Indicial Aerodynamic Responses Using Computational Aerodynamics Techniques*, Journal of Aircraft, 2008.

[30] Marques, A., Simões, C., & Azevedo, J., *Unsteady aerodynamic forces for aeroelastic analysis of two-dimensional lifting surfaces*, Journal of the Brazilian Society of Mechanical Sciences and Engineering, Vol. 28, No. 4, 2006.

[31] Billings, S., *Nonlinear system identification: NARMAX methods in the time, frequency, and spatio-temporal domains*, John Wiley & Sons, 2013.

[32] Debnath, J., *N-dimensional Laplace transforms with associated transforms and boundary value problems*, Doctoral Dissertation Iowa State University, 1988.

[33] Jain, A. K., *Fundamentals of digital image processing*, Prentice-Hall, Inc., 1989.

[34] Corinthios, M., *Signals, systems, transforms, and digital signal processing with MATLAB*, CRC Press, 2009.

[35] Bedrosian, E., and Rice, S. O., *The output properties of Volterra systems (nonlinear systems with memory) driven by harmonic and Gaussian inputs*, Proceedings of the IEEE, Vol. 59, No. 12, 1971.

[36] Mircea, A., and Sinnreich, H., *Distortion noise in frequency-dependent nonlinear networks*, Proceedings of the Institution of Electrical Engineers, Vol. 116, No. 10, IET Digital Library, 1969.

[37] Steinwolf, A., *Random Vibration Testing Beyond PSD Limitations*, Journal of Sound and Vibration, Vol. 40, No. 9, 2006.

[38] Barbati, M., Ricci, S., Climent, H., and Guitian, M. R., *Continuous Turbulence Design Loads Calculation in Presence of Non-linear Controls*, IFASD, Bristol (United Kingdom), 2013.

[39] Hoblit, F. M., *Gust loads on Aircraft: Concepts and Applications*, AIAA Education Series, 1988.

[40] Teufel, P., and Kruse, M., *Efficient Method for Coupling Discrete Gust Loads Analysis in the Frequency Domain with a Fully Non-Linear Flight Control System Simulation*, IFASD, Stockholm (Sweden), 2007.

[41] European Aviation Safety Agency, *Certification Specifications for Large Aeroplanes CS-25, Subpart C*, 2010.

[42] MSC Nastran, *Aeroelastic Analysis User's Guide Version 68*, 2002.

[43] Scott, R. C., Pototzky, A. S., and PERRY, III, B. O. Y. D., *Computation of maximized gust loads for nonlinear aircraft using matched-filter-based schemes*, Journal of Aircraft, Vol. 30, No. 5, 1993.

COPYRIGHT STATEMENT